Hindawi
Advances in Materials Science and Engineering
Volume 2019, Article ID 9807975, 11 pages
https://doi.org/10.1155/2019/9807975

*Research Article*

# Investigation and Improvement of Bursting Force Equations in Posttensioned Anchorage Zone

**Young Hak Lee and Min Sook Kim**

*Architectural Engineering, Kyung Hee University, Yongin 17104, Republic of Korea*

Correspondence should be addressed to Min Sook Kim; kimminsook@khu.ac.kr

Received 19 February 2019; Revised 6 June 2019; Accepted 2 July 2019; Published 31 July 2019

Academic Editor: José António Fonseca de Oliveira Correia



In posttensioned concrete members, the high local stress under the anchorage causes transverse tensile stress. Therefore, it is very important to predict the bursting force to determine appropriate reinforcement details. In the present work, the existing equations of the bursting force for the anchorage zone were evaluated and an equation for the bursting force based on finite element analysis was proposed to improve the model's accuracy. Parametric analysis was performed considering the anchorage shape, tendon angle, and eccentric distance. The analytical results indicate that the existing equations underestimate or overestimate the bursting force. The proposed equation is able to predict the bursting force reasonably well for an anchorage zone with rectangular bearing plate, cavity, and eccentric distance.

## 1. Introduction

Posttensioned concrete structures are widely used in architectural and civil engineering due to their high tensile capacity and crack control. In posttensioned concrete members, the concentrated prestressing force is transferred from the prestressing tendon onto the concrete via the anchorage system. Therefore, a large bearing stress is generated in the axial direction of the concrete member around the bearing plate and a tensile stress is generated in the vertical direction of the tendons. This tensile stress is called a bursting force. The bursting force should be resisted by properly designed reinforcement. The capability of the anchorage zone is one of the key factors of the safety and stability of posttensioned concrete structures. Accurate prediction of bursting stress and proper reinforcement design are required in the anchorage zone. Therefore, numerical and experimental methods have been studied by many researchers.

Mörsch [1] proposed a load path model and bursting force equation using a simplified two-dimensional strut-and-tie model. Guyon [2] proposed a simplified method based on the classical theory of elasticity for stress distribution within the anchorage zone. The magnitude and distribution of the bursting stress were investigated considering the ratio of the height of the member to the height of the bearing plate. Sahoo et al. [3] modified Guyon's equation to apply the compression-dispersion model (CDM) to the stress distribution. He and Liu [4] presented a method for determining the bursting force based on individual formulations of compression-dispersion models considering concentric, eccentric, and inclined tendons. Zhou et al. [5] proposed a mathematical model in order to predict the bursting force and the distribution of transverse stress in the anchorage zone. This method was verified by the results of finite element simulations. Hou et al. [6] performed finite element analysis to evaluate the validity of the strut-and-tie model used in existing research. Eccentric distance and size of the bearing plate were considering as variables. A modified strut-and-tie model was proposed to predict the bursting force using separate cases for small and large eccentric distances.

Few investigations have been performed to evaluate the efficiency of the bottle-shaped strut method. Yuan et al. [7] performed the bottle-shaped strut method to evaluate the effects of the concentration ratio and rotation angle of

reinforcement. The results show that as the concentration ratio increases, the dispersion angle decrease and that as the rotation angle increases, the efficiency coefficient increases in the bottle-shaped strut method. Sahoo and Varghese [8] investigated the effect of lateral confinement on the efficiency of bottle-shaped struts. Arabzadeh et al. [9] investigated the efficiency factors and proposed model for the prediction of the efficiency factor of concrete strength-based modified compression field theory. Campione and Minafò [10] studied on bottle-shaped struts and members based on the structural tests. They proposed the model to evaluate the ultimate capacity of specimens.

Although some new methodologies have been developed, the anchorage shape, tendon angle, and eccentricity are still not considered in the bursting force equation. In the present work, a bursting force equation is proposed based on the results of finite element analysis. The analytical results were used to evaluate the bursting force equations including the proposed equation, Mörsch, Guyon, Zhou, and AASHTO [1, 2, 5, 11].

## 2. Bursting Force Equation

The approaches that have been used to determine a bursting force equation have included the strut-and-tie model, analysis using theory of elasticity, and finite element models. Mörsch [1] had studied the bursting force using a simplified two-dimensional strut-and-tie model, as shown in Figure 1. This equation can account for the ratio of the height of the concrete section to the height of the bearing plate. It is assumed that the maximum bursting stress occurs at half the depth of the cross section and the factor $k$ is 0.5:

$$F_{\text{bst,Mörsch}} = \frac{P}{2}\tan\theta = \frac{P}{2}\frac{1}{kh}\left(\frac{h}{4}-\frac{a}{4}\right) = 0.25P\left(1-\frac{a}{h}\right), \tag{1}$$

where $P$ is the applied tendon load, $\theta$ is the angle between the strut and tie, $a$ is the width of the bearing plate, $h$ is the depth of the cross section, and $k$ is a factor that accounts for the point at which the maximum bursting stress occurs.

Guyon [2] used isostatic lines of compression (ILCs) to visualize the flow of forces in the anchorage zone, as shown in Figures 2(a) and 2(b). Experiments were conducted using the ratio of the size of the bearing plate to the width of the member as variables. Based upon the test results, a bursting force equation was proposed as shown in equation (2), where $k$ is assumed to be 0.4. When the tendon force is applied eccentrically on the member, the tendon load is assumed to act on a symmetrical prism. The concept of symmetrical prism can also be applied to the following equation:

$$F_{\text{bst,Guyon}} = \frac{1}{8k}P\left(1-\frac{a}{h}\right) = 0.30P\left(1-\frac{a}{h-2e}\right), \tag{2}$$

where $P$ is the tendon load, $a$ is the width of the bearing plate, $h$ is the depth of the cross section, and $e$ is the eccentricity.

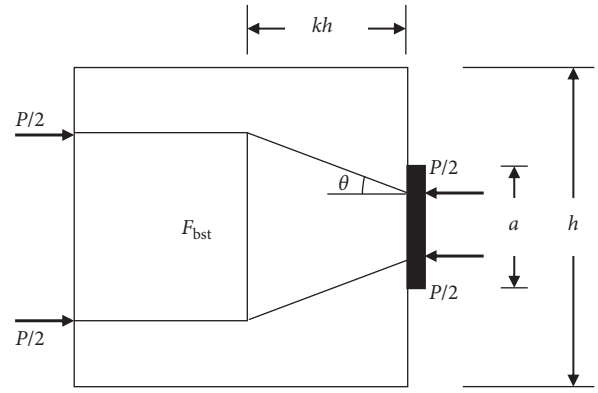


$P$ : tendon load
$\theta$ : angle between struct and and tie
$a$ : width of bearing plate
$h$ : depth of cross section
$k$ : location coefficient to define where max. burting force occurs

Figure 1: Strut-and-tie model (reproduced from Mörsch [1], under the Creative Commons Attribution license/public domain).

AASHTO [11] has used the Burdet [12] equation since 1994. Based on the geometrical shape, Burdet [12] proposed a bursting force equation that accounts for inclined tendons, as shown in the following equation:

$$F_{\text{bst,AASHTO}} = 0.25\sum P\left(1-\frac{a}{h}\right) + 0.5\sum(P\sin\alpha), \tag{3}$$

where $P$ is the applied tendon load, $a$ is the width of the bearing plate, $h$ is the depth of the cross section, and $\alpha$ is the tendon angle.

He and Liu [4] proposed a bursting force equation for different loading conditions, while the AASHTO equation is found to be overly conservative in most cases. The compression-dispersion model was established and proposed $h/3$ as the starting point of integration to consider the occurrence of large bearing stress near the bearing plate. The bursting force equation was obtained by integrating the transverse tensile stress along the tendon path as shown in the following equations:

$$F_{\text{bst,1}} = \int_{h/3}^{h}\sigma_T dx = \frac{2}{9}P\left(1-\frac{a}{h}\right), \tag{4}$$

$$F_{\text{bst,He}} = 0.22\sum P(1+\gamma)^2\left(1-\gamma-\frac{a}{h}\right) + 0.5\sum P\sin\alpha\left(1-\frac{a}{h}\right), \tag{5}$$

where $h$ is the depth of the cross section, $\sigma_T$ is the transverse stresses along the tendon path, $P$ is the applied tendon load, $a$ is the width of the bearing plate, $\gamma$ is the eccentric ratio of tendons, which can be expressed as $2e/h$, and $e$ is the eccentric distance.

Zhou et al. [5] evaluated the equations of He and Liu [4] and AASHTO [11] by comparing them with the results of finite element analysis. The bursting force coefficient was

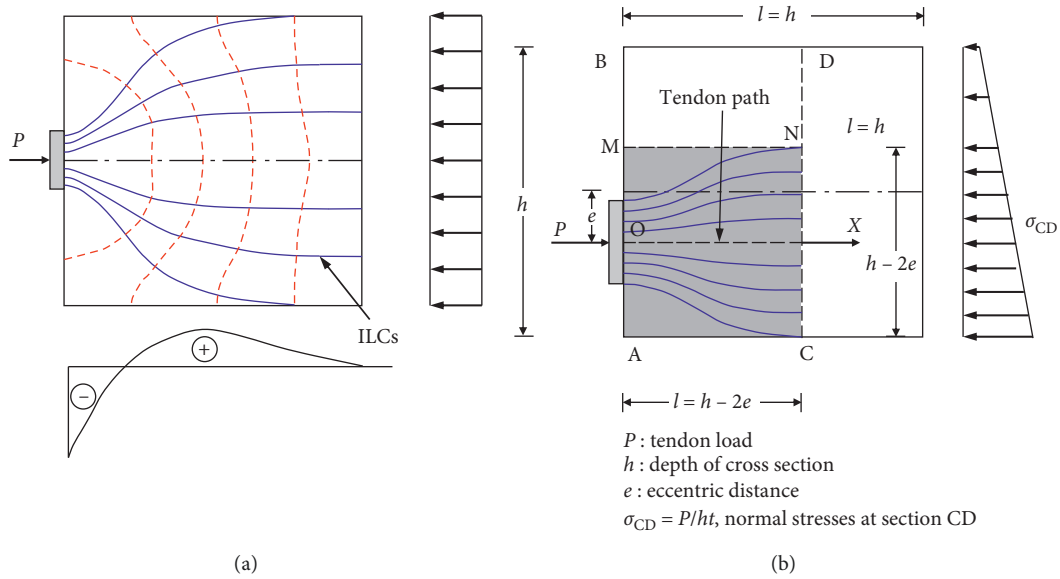


Figure 2: Isostatic lines of compression (reproduced from Guyon [2], under the Creative Commons Attribution license/public domain). (a) Centric and (b) eccentric.

modified from 0.22 to 0.25 based on the results of the finite element analysis. Also, equation (6) was proposed considering the tendon angle and eccentricity using the symmetrical prism method as shown in Figure 3:

$$F_{\text{bst,Zhou}} = 0.25P(1+\gamma)^2\left(1-\gamma-\frac{a}{h}\right)+0.5P\sin\alpha\left(1-\frac{a}{h}\right), \tag{6}$$

where $P$ is the applied tendon load, $\gamma$ is the eccentric ratio of tendons, which can be expressed as $2e/h$, $e$ is the eccentric distance, $h$ is the depth of the cross section, $a$ is the width of the bearing plate, and $\alpha$ is the angle of the tendon.

Table 1 shows a comparison between different methods for the calculation of bursting forces, including the equations of Mörsch, Guyon, Zhou, and AASHTO [1, 2, 5, 11].

## 3. Finite Element Analysis

*3.1. Finite Element Model.* The bursting force was analyzed based on finite element simulation to evaluate the effect of the anchorage shape, tendon angle, and eccentricity. The commercial structural analysis software ANSYS 15.0 was used to analyze the bursting force. The solid element was used for modelling an analytical model. This element is defined by eight nodes having three degrees of freedom at each node: translations in the nodal $x$, $y$, and $z$ directions. Cracks and crushing of the concrete were not considered because it is the purpose of the analysis to evaluate the magnitude and distribution of the bursting stress. The automesh function in ANSYS was used to generate solid elements to model anchorage and concrete blocks. The load step sizes were controlled using an automatic time stepping. The convergence was checked using the Newton–Raphson iterations at every loading step.

The analytical model size was determined according to the specimen specification of the load transfer test standard

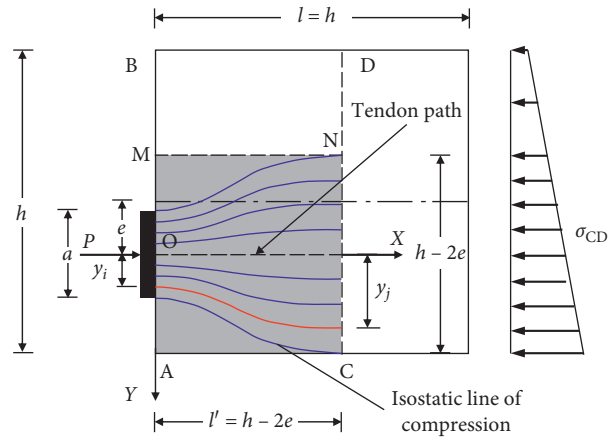


Figure 3: The symmetrical prism approach in the eccentric anchorage zone (reproduced from Zhou et al. [5], under the Creative Commons Attribution license/public domain).

described in ETAG 013 [13]. In order to minimize the influence of the bearing plate area, all of the analytical models have the same area. The compressive strength and the tensile strength of the concrete were 40 MPa with a peak strain of 0.0025. The constitutive model used is the model developed by Saenz [14]. The tensile stress is 4 MPa. The yield strength of the anchorage was 450 MPa. In this study, the perfectly elastic-plastic criterion material was used for anchorage. The force is applied as a uniform load within the footprint of the anchor plate and prestressing tendons are not modelled [5].The applied load was performed as a static load at the bearing plate as shown in Figures 4(a)–4(c). The anchorage

Table 1: Comparison of different bursting force equations.

| Code | Bursting force equation | Factors included in the equations | | |
|---|---|---|---|---|
| | | Anchorage shape | Eccentricity | Inclined duct |
| Mörsch | $0.25P(1-(a/h))$ | × | × | × |
| Guyon | $0.30P(1-(a/h))$ | × | ○ | × |
| AASHTO | $0.25\sum P(1-(a/h))+0.5\sum(P\sin\alpha)$ | × | × | ○ |
| Zhou | $0.25P(1+\gamma)^2(1-\gamma-(a/h))+0.5P\sin\alpha(1-(a/h))$, where $\gamma=2e/h$ | × | ○ | ○ |

$P$: tendon load; $\gamma$: eccentric ratio of tendons; $h$: depth of the cross section; $a$: width of the bearing plate; α: angle of tendon; $e$: eccentricity.

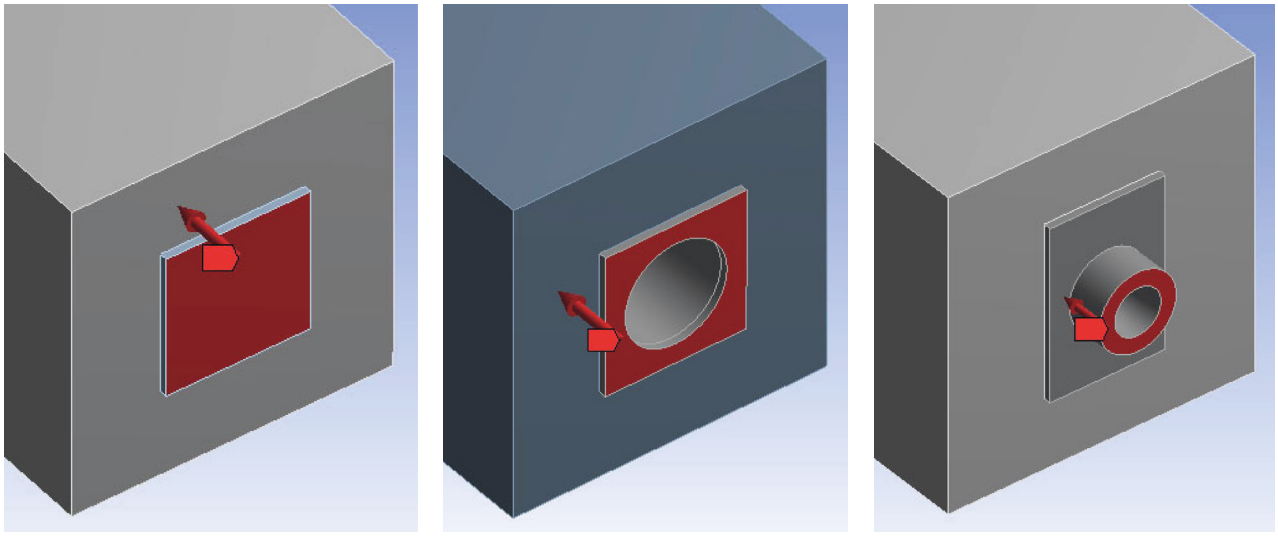

(a) (b) (c)

Figure 4: Dimension and loading on the bearing plate. (a) Model S, (b) Model C, and (c) Model A.

and concrete were set to perfect bonded option. The virtual path was set in the analytical model to measure the bursting stress, as shown in Figure 5. In the analytical model without a cavity, the virtual path was set at the center of the model as shown in Figure 5(a). In the model with a cavity, the virtual path was set between the concrete and cavity as shown in Figures 5(b) and 5(c).

To verify the analytical model, an experiment was carried out where a concrete specimen of 250 mm × 250 mm × 600 mm in size was tested, as shown in Figure 6. The compressive strength of the concrete was 40 MPa. The initial stiffness of the analytical model was slightly larger than the experimental data. It is concluded that the reduction of the stiffness was not considered due to the concrete crack in the analytical model. However, results show that the test ultimate load of the specimen is 722.3 kN. Using the analytical model, the predicted ultimate load is 745.2 with a reasonable error of about 4% compared with the test failure load. Therefore, the analytical model is appropriate for the prediction of the bursting force.

*3.2. Parametric Analysis.* The anchorage shape, the tendon angle, and the eccentric distance were considered as variables in a finite element analysis, as shown in Figure 7. In order to evaluate the effect of the anchorage shape on bursting stress, square bearing plate without cavity, square bearing plate with cavity, and rectangular bearing plate with protruding cavity were modelled as shown in Figure 7(a). The dispersion of compression is influenced by the bearing area of the applied load (Sahoo et al. [3]). The three models have a similar bearing area to minimize the influence of the bearing plate area. In this paper, two tendon angles were considered: 0° and 5° as shown in Figure 7(b). The position of the anchorage moved to consider the eccentric distance, as shown in Figure 7(c). The eccentric distance was increased by 40 mm. Table 2 lists the related parameters used in the finite element analysis.

The load of 100% of the ultimate load of the tendon was applied to on top of the bearing plate. The bursting force was calculated by plotting the stress measured in the virtual path and multiplying the area of the graph by the width of the member, as shown in Figure 8. This method was proposed by Stone [15] and used the following equation:

$$F_{\text{bst}} = \int \sigma_{\text{bst}} t\, dx, \tag{7}$$

where $\sigma_{\text{bst}}$ is the bursting stress and $t$ is the width of the member.

## 4. Proposed Bursting Force Equation

Figures 9(a) and 9(b) show the distribution of the bursting stress according to the anchorage shape. The maximum bursting stress of Model A, using a square bearing plate, was

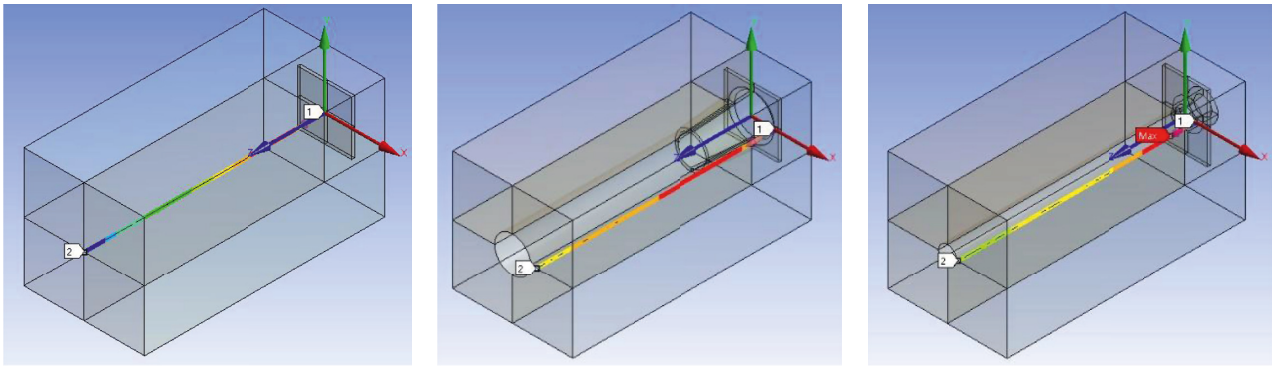

(a) (b) (c)

Figure 5: Virtual path across the tendon. (a) Model S, (b) Model C, and (c) Model A.

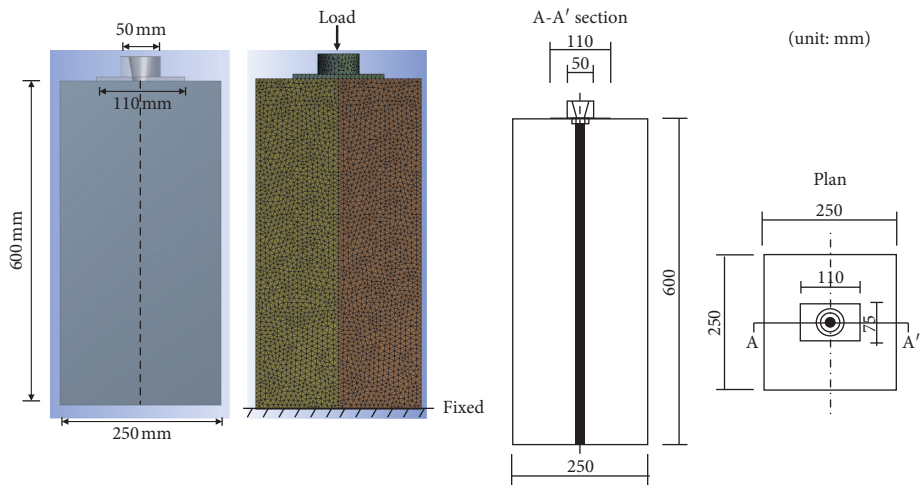


(a) (b)

(c) (d)

Figure 6: Continued.

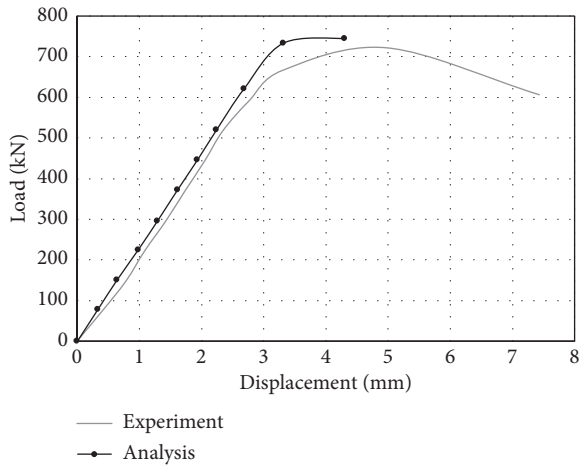


(e)

Figure 6: Comparison of finite element analysis result and experiment result. (a) Finite element model. (b) Dimension of the specimen. (c) Test setup. (d) Failure of the specimen. (e) Comparison of the load-displacement curve.

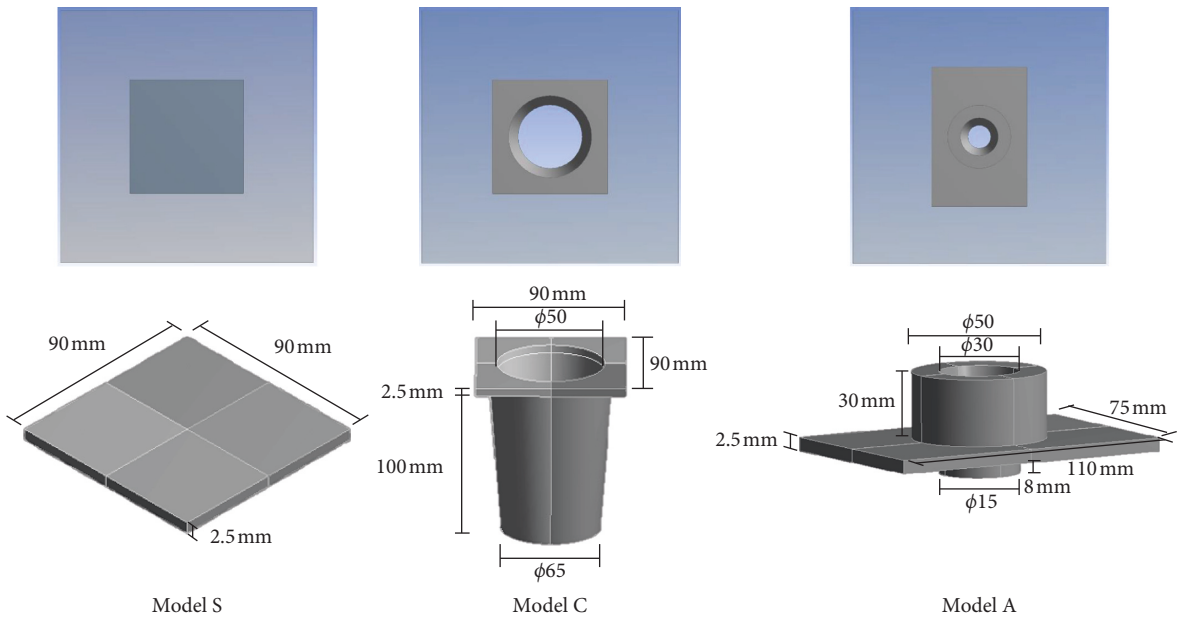


(a)

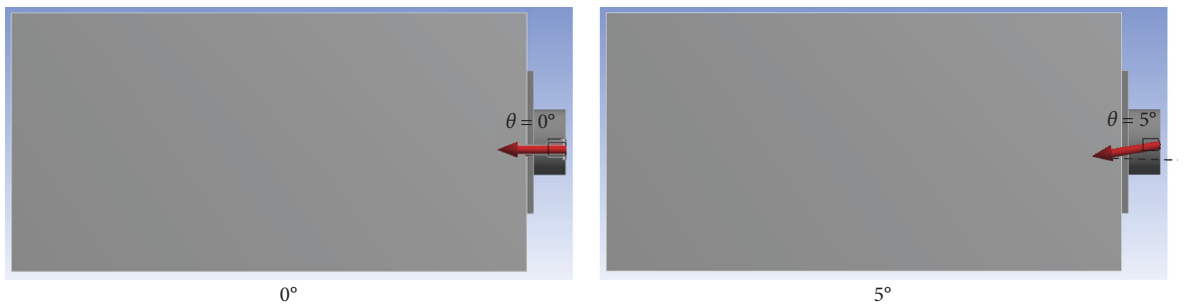


(b)

Figure 7: Continued.

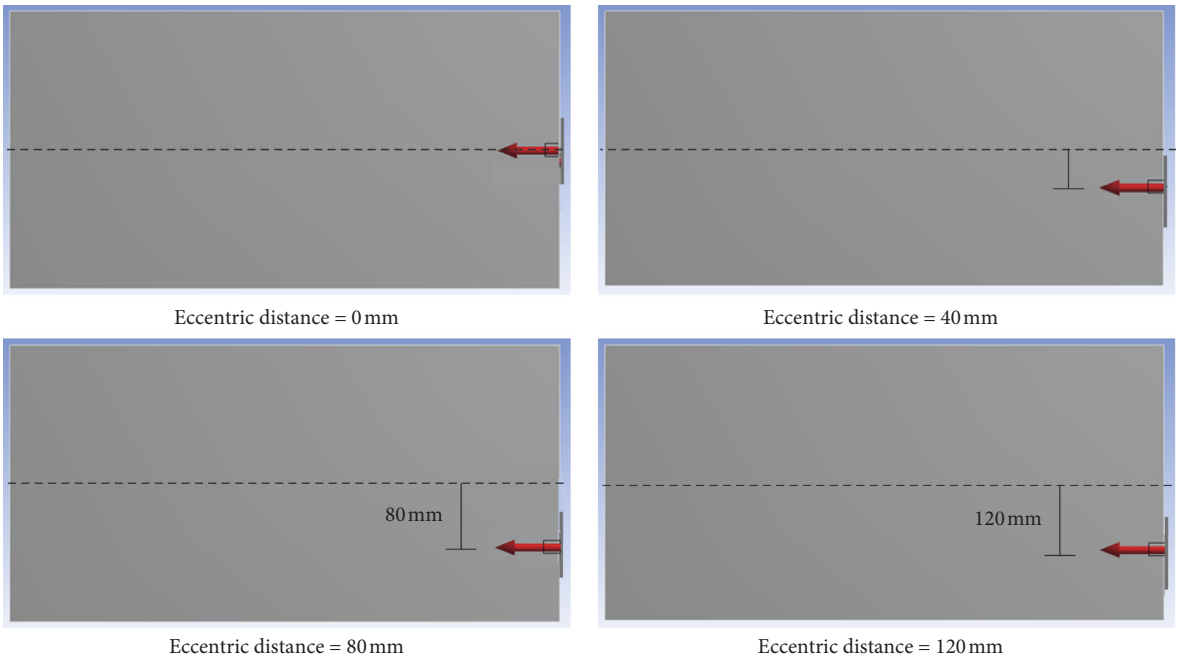


(c)

Figure 7: Variables for the finite element analysis model. (a) Anchorage shape. (b) Angle of the tendon. (c) Eccentric distance.

Table 2: Parameters for the finite element analysis.

| Variables | Details | Model |
|---|---|---|
| Anchorage shape | Square bearing plate without cavity | S |
| | Square bearing plate with cavity | C |
| | Rectangle bearing plate with cavity | A |
| Angle of tendon | 0° | — |
| | 5° | I |
| Eccentricity | Eccentric distance 0 | SE0 |
| | Eccentric distance 40 mm | SE40 |
| | Eccentric distance 80 mm | SE80 |
| | Eccentric distance 120 mm | SE120 |

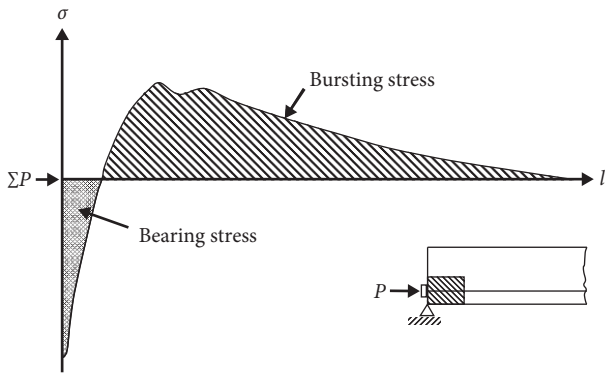


Figure 8: Method used for bursting force calculation.

measured to be 3.3 times larger than that of the other models. The bursting stress of the square bearing plate was uniformly distributed, whereas that of the rectangular bearing plate was relatively concentrated in the long side direction. It is concluded that the stress distribution varies depending on the anchorage shape.

As shown in Figures 10(a)–10(c), bursting stress occurred along the direction of the tendon in the anchorage zone. In Model A, the stress was concentrated or distributed along the tendon, but in Model C with cavity, the stress was concentrated at the joint of the cavity and the duct. The maximum bursting stress of the model with the cavity occurred farther from the surface of the concrete member than did the model without the cavity, as shown in Figure 9. In Model S without the cavity, the applied load was transferred from the bearing plate to the concrete. On the other hand, in Model C with cavity, the applied load was transferred from the bearing plate to the cavity and from the cavity to the concrete. The angle of the tendon did not affect the position and magnitude of the maximum bursting stress. However, the overall stress distribution was different. In the case of 0° of tendon angle, the stress was mainly distributed at the joint of the cavity and the duct, whereas the stress was distributed more widely in the 5° tendon angle model. The finite element analysis results indicated that the magnitude of the bursting stress decreases as the eccentric distance increases. The bursting forces of all analytical models are summarized in Table 3.

Based on the results of the finite element analysis and Guyon's equation, a bursting force equation considering the anchorage shape, tendon angle, and eccentricity was proposed to improve the accuracy of the bursting force prediction. The aspect ratio of the anchorage and the cavity length were proposed to consider the anchorage shape. The proposed bursting force equation can be expressed as

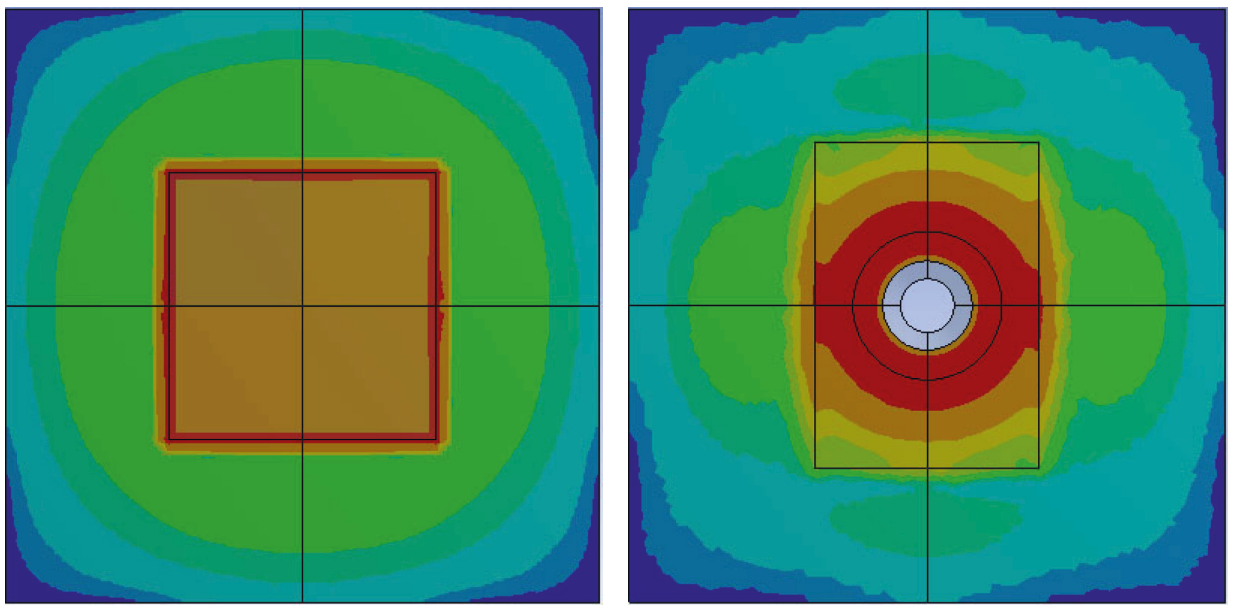

(a) (b)

Figure 9: Comparison of von Mises stress depending on the anchorage shape. (a) Model S and (b) Model A.

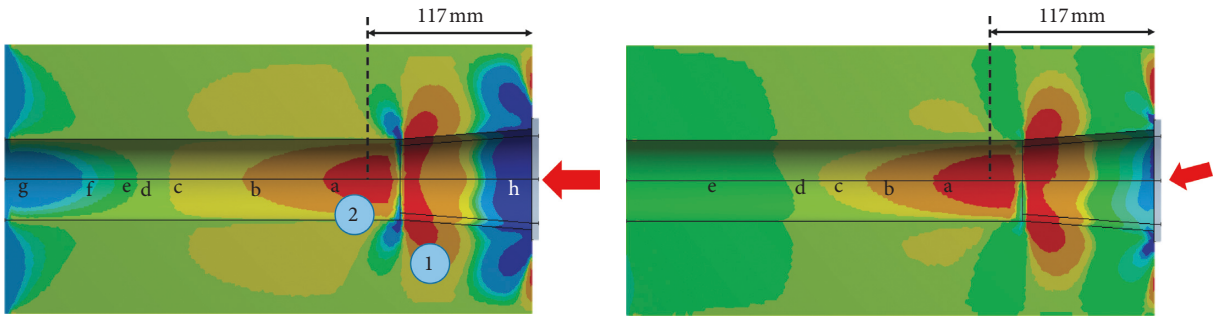


a: 1.5~3.98 MPa
b: 0.5~1.5 MPa
c: 0~0.5 MPa
d: −0.2~0 MPa
e: −0.4~0.2 MPa
f: −0.6~0.4 MPa
g: −0.8~0.6 MPa
h: −47~0.8 MPa

(a)

a: 1.3~5.54 MPa
b: 0.5~1.3 MPa
c: 0.2~0.5 MPa
d: 0~0.2 MPa
e: −2~0 MPa

(b)

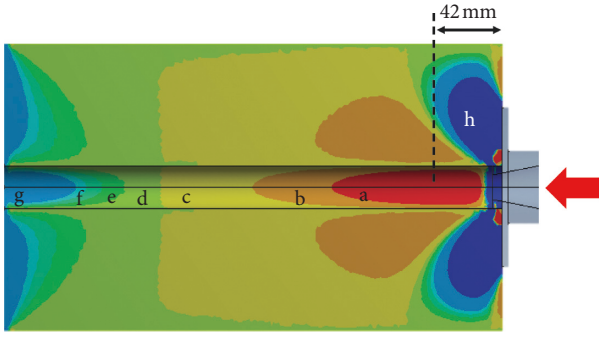


a: 2~7.93 MPa
b: 0.5~2 MPa
c: 0~0.5 MPa
d: −0.2~0 MPa
e: −0.4~0.2 MPa
f: −0.6~0.4 MPa
g: −0.8~0.6 MPa
h: −2~0.8 MPa

(c)

Figure 10: Comparison of normal stresses to investigate the effect of the wedge cavity. (a) Model C, (b) Model CI, and (c) Model A.

Table 3: Bursting forces and variables.

| | S | C | A | SI | CI | AI | SE0 | SE40 | SE80 | SE120 |
|---|---|---|---|---|---|---|---|---|---|---|
| $h$ (mm) | 200 | | | | | | 400 | | | |
| $t$ (mm) | 200 | | | | | | | | | |
| $\alpha$.(mm) | 90 | 90 | 110 | 90 | 90 | 110 | 90 | | | |
| $\alpha$ (°) | 0 | | | 5 | | | 0 | | | |
| $e$ (mm) | 0 | | | | | | 0 | 40 | 80 | 120 |
| $P$ (kN) | 258 | | | | | | | | | |
| $k[=(l/h)]$ | 0.375 | 0.375 | 0.208 | 0.375 | 0.375 | 0.208 | 0.291 | 0.314 | 0.347 | 0.416 |
| $F_{bst}/t$ (N/mm) | 169.0 | 187.2 | 552.9 | 166.4 | 328.1 | 540.6 | 211.7 | 200.0 | 163.6 | 139.9 |
| $F_{bst}$ (kN) | 33.8 | 37.4 | 110.6 | 33.3 | 65.6 | 108.1 | 42.3 | 40.0 | 32.7 | 28.0 |

$$F_{bst,proposed} = \Phi K P\left(1 - \frac{a_1}{h - 2e}\right) + \left(\frac{h}{h - l_{in}}\right)0.5P \sin\alpha, \quad (8)$$

$$K = \frac{1}{8k\beta_a}, \quad k < 0.3, \quad (9a)$$

$$K = 0.25, \quad k \geq 0.3, \quad (9b)$$

$$\beta_a = \frac{a_2}{a_1}, \quad a_1 \geq a_2, \quad (10a)$$

$$\beta_a = 1, \quad a_1 < a_2, \quad (10b)$$

$$\Phi = 0.5\left(\frac{h}{h - e}\right), \quad e \neq 0, \quad (11a)$$

$$\Phi = 1, \quad e = 0, \quad (11b)$$

where $\Phi$ is the eccentric distance coefficient, $K$ is the anchorage shape factor, $h$ is the height of the cross section of the concrete, $e$ is the eccentric distance, $a_1$ is the vertical length of the bearing plate, $a_2$ is the horizontal length of the bearing plate, $l_{in}$ is the length of the cavity embedded in the concrete, $k$ is the ratio of a point where maximum bursting stress occurs to $h$, and $\beta_a$ is the aspect ratio of the anchorage, not to exceed 1.

## 5. Evaluation of the Proposed Equation

The proposed equation was compared with the existing equations in order to identify which proposed equation is able to provide the most accurate estimate of the bursting force. The bursting force equations were evaluated in terms of anchorage shape, angle of tendons, and eccentric distance.

Table 4 shows the results of the comparison between the results of the finite element analysis and the bursting force equations. Figure 11 shows the bursting force according to the shape of the anchorage. The existing equations underestimated the bursting force of Model A (rectangular shape) because they did not consider the aspect ratio of the bearing plate. The proposed equation considers the aspect ratio of the bearing plate and predicts the bursting force relatively well.

Table 4: Evaluation of the bursting force equations' accuracy.

| Equation | Mean | Standard deviation | Error (%) |
|---|---|---|---|
| Mörsch | 0.971 | 0.53 | 50 |
| Guyon | 0.990 | 0.46 | 37.5 |
| AASHTO | 1.005 | 0.50 | 50 |
| Zhou | 0.895 | 0.43 | 50 |
| Proposed | 1.056 | 0.12 | 25 |

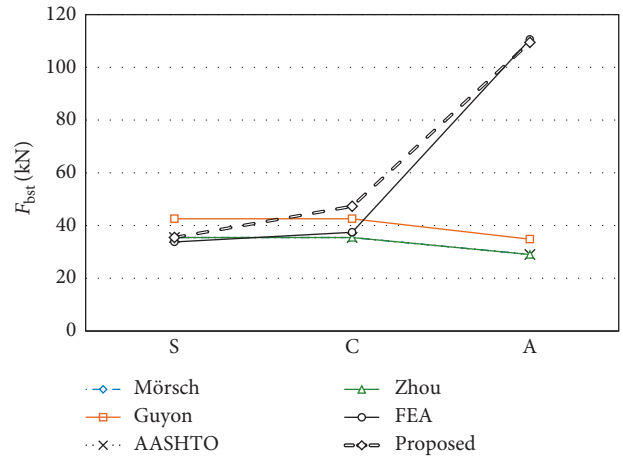


Figure 11: Evaluation of the proposed equation on the anchorage shape.

The results of the finite element analysis indicate that Model S has no difference in bursting force according to the tendon angle, but Models A and C have increased bursting force when the tendon angle is 5°. It is concluded that the consideration of the cavity affects the bursting force according to the tendon angle. Figure 12 shows the bursting force according to the tendon. In the case of Model A (without cavity), all equations well predicted comparatively the bursting force. However, in Models A and C (with cavities), the existing equations underestimated the bursting force. The equation of AASHTO [11] and Zhou et al. [5] underestimated the bursting force for Models C and A with cavities, even though the tendon angle was included in the equations.

In cases of large eccentric distance, the failure of the equations of AASHTO [11] and Mörsch [1] to consider eccentric distance leads to an overestimation of the bursting

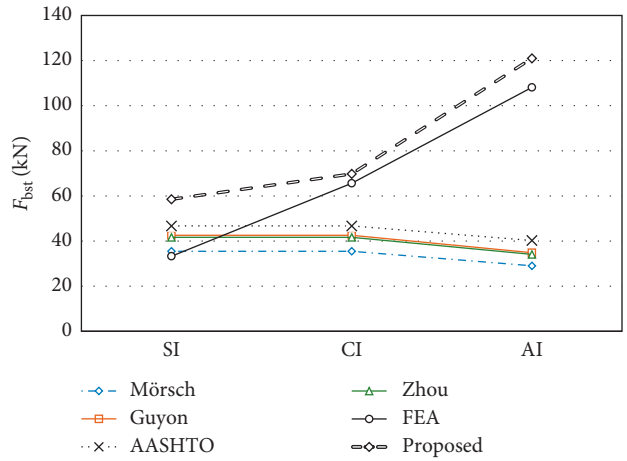


Figure 12: Evaluation of the proposed equation on the tendon angle.

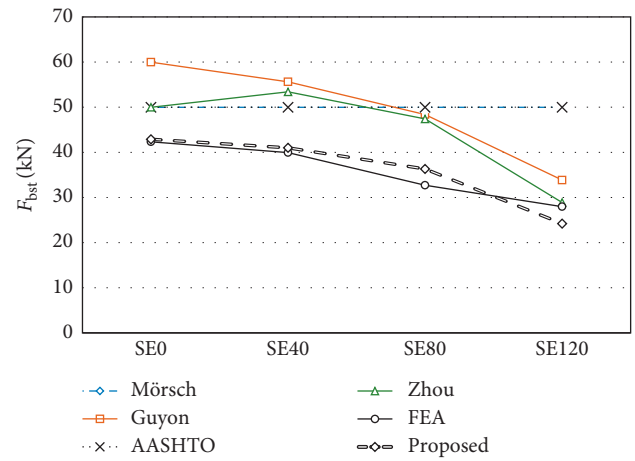


Figure 13: Evaluation of the proposed equation on the eccentric distance.

force, as shown in Figure 13. The proposed equation and the equations of Guyon [2] and Zhou et al. [5] predicted the decrease of bursting force with increasing eccentric distance. However, the equations of Guyon [2] and Zhou et al. [5] overestimated the bursting force, despite considering eccentric distance, except in the case of the 120 mm eccentric distance.

Figure 14 shows the ratios of the calculated bursting forces to the results of the finite element analysis. Existing equations underestimated the bursting force of the anchorage with rectangular bearing plate and overestimated the effect of eccentricity. The comparison results are summarized in Table 4. It is concluded that the existing equations underestimate or overestimate the bursting force depending on the parameters, whereas the proposed equation provides reasonable predictions.

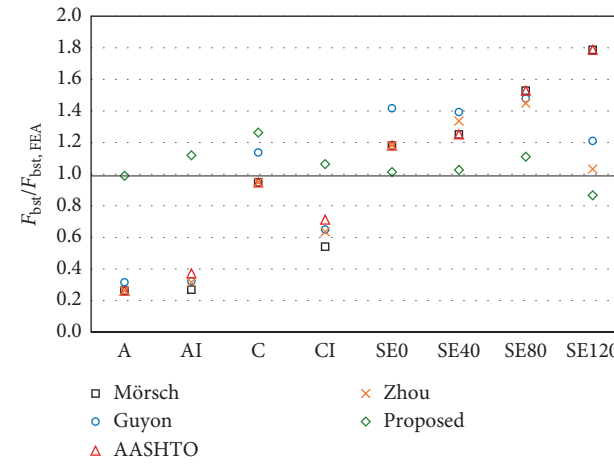


Figure 14: Evaluation of the proposed bursting force equation.

## 6. Conclusions

In this paper, a bursting force equation was proposed to improve the accuracy of bursting force calculations. A finite element analysis was performed considering the anchorage shape, tendon angle, and eccentricity as variables to verify the proposed equation. The following conclusions can be made:

(1) The results of the finite element analysis indicated that the rectangular bearing plate had a relatively concentrated stress on the long side of the plate. Therefore, an anchorage shape factor considering the aspect ratio of the bearing plate was proposed.

(2) In the case of the anchorage considering the cavity, the bursting force showed a large difference according to the tendon angle. The function of the embedded length of the cavity was considered in the bursting force equation. Also, as the eccentric distance increases, the bursting force decreases. This is considered in the eccentric distance coefficient.

(3) Parametric analysis was carried out with the anchorage shape, tendon angle, and eccentric distance to evaluate the bursting force equations, including the proposed equation. The proposed equation shows a reasonable prediction of the bursting force of the anchorage with a rectangular bearing plate, whereas the existing equations underestimated this value because they did not consider the aspect ratio of the bearing plate.

(4) For an analytical model without a cavity, all bursting force equations performed well. However, in the analytical model with cavity, the existing equations underestimated the bursting force. The proposed equation predicted the bursting force considering the tendon angle more accurately.

(5) Mörsch and AASHTO did not predict the bursting stress due to changes in eccentric distance because the eccentric distance is not considered in the bursting force equation, while Guyon and Zhou predicted the bursting force relatively well for large eccentricity. However, it tends to be overestimated for small eccentricity. The proposed equation

accurately predicted the bursting force regardless of the eccentric distance.

## Data Availability

The data used to support the findings of this study are available from the corresponding author upon request.

## Conflicts of Interest

There are no conflicts of interest regarding the publication of this paper.

## Acknowledgments

This work was supported by the National Research Foundation of Korea (NRF) grant funded by the Korea Government (MSIT) (NRF-2017R1A2B2005581).

## References

[1] E. Mörsch, "über die berechnung der gelenkquader," *Beton-und-Eisen*, vol. 23, no. 12, pp. 156–161, 1924.

[2] Y. Guyon, *Prestressed Concrete*, Contractors Record and Municipal Engineering, London, UK, 1953.

[3] D. K. Sahoo, B. Singh, and P. Bhargava, "Investigation of dispersion of compression in bottle-shaped struts," *ACI Structural Journal*, vol. 106, no. 2, pp. 178–186, 2009.

[4] Z.-Q. He and Z. Liu, "Investigation of bursting forces in anchorage zones: compression-dispersion models and unified design equation," *Journal of Bridge Engineering*, vol. 16, no. 6, pp. 820–827, 2011.

[5] L.-Y. Zhou, Z. Liu, and Z.-Q. He, "Further investigation of transverse stresses and bursting forces in post-tensioned anchorage zones," *Structural Concrete*, vol. 16, no. 1, pp. 84–92, 2015.

[6] D.-W. Hou, J.-L. Zhao, J. S.-L. Shen, and J. Chen, "Investigation and improvement of strut-and-tie model for design of end anchorage zone in post-tensioned concrete structure," *Construction and Building Materials*, vol. 136, pp. 482–494, 2017.

[7] A. Yuan, S. Qian, and H. Dai, "Effects of design parameters on behaviour in bottle-shaped struts," *Magazine of Concrete Research*, pp. 1–34, 2019.

[8] D. K. Sahoo and B. P. Varghese, "Effect of confinement on the efficiency of bottle-shaped struts," *Magazine of Concrete Research*, pp. 1–10, 2018.

[9] A. Arabzadeh, R. Aghayari, and A. R. Rahai, "A new model for predicting the effective strength in reinforced concrete bottle-shaped struts," *International Journal of Civil Engineering*, vol. 10, no. 4, pp. 253–262, 2012.

[10] G. Campione and G. Minafò, "Experimental investigation on compressive behavior of bottle-shaped struts," *ACI Structural Journal*, vol. 108, no. 3, pp. 294–303, 2011.

[11] AASHTO, *LRFD Bridge Design Specifications*, American Association of State Highway & Transportation Officials, Washington, DC, USA, 5th edition, 2010.

[12] O. Burdet, *Analysis and design of anchorage zone in post-tensioned concrete bridges*, Ph.D. dissertation, The University of Texas at Austin, Austin, TX, USA, 1990.

[13] EOTA, *ETAG 013 Guideline for European Technical Approval of Post-tensioning Kits for Prestressing of Structures*, European Organisation for Technical Approvals, Brussels, Belgium, 2002.

[14] L. P. Saenz, "Discussion of Equation for the stress-strain curve of concrete," *Journal of American Concrete Institute*, vol. 61, no. 9, pp. 1229–1235, 1964.

[15] W. C. Stone, *Design criteria for post-tensioned anchorage zone tensile stresses*, Ph.D. dissertation, The University of Texas at Austin, Austin, TX, USA, 1980.